Repository of the Max Delbrück Center for Molecular Medicine (MDC) in the Helmholtz Association

Skin sodium measured with (23) Na MRI at 7.0 T.

Linz, P., Santoro, D., Renz, W., Rieger, J., Ruehle, A., Ruff, J., Deimling, M., Rakova, N., Muller, D.N., Luft, F.C., Titze, J., Niendorf, T.

Skin sodium measured with 23Na magnetic resonance imaging at 7.0 Tesla

Skin sodium measured with [23]Na magnetic resonance imaging at 7.0 Tesla

Peter Linz, PhD [1]; Davide Santoro, PhD [2]; Wolfgang Renz, PhD [3]; Jan Rieger, MSc [2]; Anjuli Ruehle, MSc [2]; Jan Ruff, PhD [3]; Michael Deimling, PhD [3]; Natalia Rakova, MD [5]; Dominik N. Muller, PhD [5,6]; Friedrich C. Luft, MD [5]; Jens Titze, MD [1,7]; and Thoralf Niendorf, PhD [2]

[1]Interdisciplinary Center for Clinical Research, Nikolaus-Fiebiger-Center for Molecular Medicine, Friedrich-Alexander-University Erlangen-Nürnberg, Germany

[2]Berlin Ultrahigh Field Facility, Max-Delbrueck Center for Molecular Medicine, Berlin, Germany

[3]Siemens Healthcare, Erlangen, Germany

[4]Department of Experimental Medicine I, Nikolaus-Fiebiger-Center for Molecular Medicine, Friedrich-Alexander-University Erlangen-Nürnberg, Germany

[5]Experimental and Clinical Research Center, a joint cooperation between the Charité Medical Faculty and the Max-Delbrueck Center for Molecular Medicine, Berlin, Germany

[6]Max-Delbrueck Center for Molecular Medicine, Berlin, Germany

[7]Division of Clinical Pharmacology, Vanderbilt University School of Medicine, Nashville, USA

Correspondence:
Prof. Dr. Thoralf Niendorf, Ph.D.
Max Delbrueck Center for Molecular Medicine
Robert Roessle Strasse 10
13125 Berlin, Germany
phone: +49 30 9406 4505
e-mail: thoralf.niendorf@mdc-berlin.de

Short title: Skin sodium measured with ^{23}Na magnetic resonance imaging at 7.0 Tesla

Key words: magnetic resonance imaging; ultrahigh field magnetic resonance; radio frequency coil; salt; sodium; skin; hypertension; salt balance

Word count: 4960

Abstract

Objective: Skin-sodium storage, as a physiologically important regulatory mechanism for blood pressure, volume regulation, and indeed survival, has recently been rediscovered. This prompted the development of MRI methods to assess sodium storage in humans (^{23}Na-MRI) at 3.0 Tesla. This work examines the feasibility of high in-plane spatial resolution ^{23}Na MRI in skin at 7.0 T.

Methods: A two-channel transceiver RF coil array tailored for skin MRI at 7.0 T (f=78.5 MHz) is proposed. Specific absorption rate (SAR) simulations and a thorough assessment of RF power deposition were performed to meet the safety requirements. Human skin was examined in an *in vivo* feasibility study using 2D gradient echo imaging. Normal male adult volunteers (n=17, mean $\pm$ SD = 46 $\pm$ 18 years, range: 20-79 years) were investigated. Transverse slices of the calf were imaged with ^{23}Na MRI using a high in-plane resolution of (0.9 x 0.9) mm^2. Skin Na$^+$ content was determined using external agarose standards covering a physiological-range of Na$^+$ concentrations. To assess the intra-subject reproducibility, each volunteer was examined three to five times with each session including a 5 min walk and repositioning/preparation of the subject. Age-dependence of skin Na$^+$ content was investigated.

Results: The ^{23}Na RF coil provides improved sensitivity within a range of 1 cm from its surface versus a volume RF coil which facilitates high in-plane spatial resolution imaging of human skin. Intra-subject variability of human skin sodium content in the volunteer population was <10.3%. An age-dependent increase in skin Na$^+$ content was observed, r = 0.78).

Conclusions Assigning sodium stores with ^{23}Na-MRI techniques could be improved at 7.0 T compared to current 3.0 T technology. The benefits of such improvements would be in positive alignment with basic research and clinical applications that are designed to unlock questions regarding Na^+ balance and Na^+ storage function of skin.

Key words: magnetic resonance imaging; ultrahigh field magnetic resonance; radio frequency coil; salt; sodium; skin; hypertension; salt balance

List of Abbreviations

^{23}Na MRI	sodium magnetic resonance imaging
B_0	main magnetic field strengths
B_1^+	electromagnetic transmission field
EMF	electromagnetic fields
f	frequency in Hertz
FA	flip angle in degree
FLASH	Fast Low Angle Shot
FOV	field of view
FR4	copper clad sheet for electronic applications using glass-epoxy resin
IEC	International Electrical Commission
MIP	maximum intensity projection
MPS	monocyte phagocytic system
NA	number of averages
NaCl	sodium chloride
NFAT5	nuclear factor of activated T-cells 5
RF	radio frequency
SAR	signal absorption rate
SD	standard deviation
T_1	longitudinal relaxation time
T_2^*	effective transversal relaxation time
TonEBP	tonicity-responsive-enhance binding protein
TE	echo time
TR	repetition time
UHF-MR	ultrahigh field magnetic resonance
VEGF-C	vascular endothelial growth factor-C

Graphical Abstract

Skin sodium measured with [23]Na magnetic resonance imaging at 7.0 Tesla

Peter Linz, PhD [1]; Davide Santoro, PhD [2]; Wolfgang Renz, PhD [3]; Jan Rieger, MSc [2]; Anjuli Ruehle, MSc [2]; Jan Ruff, PhD [3]; Michael Deimling, PhD [3]; Natalia Rakova, MD [5]; Dominik N. Muller, PhD [5,6]; Friedrich C. Luft, MD [5]; Jens Titze, MD [1,7]; and Thoralf Niendorf, PhD [2]

Short abstract

This work demonstrates the feasibility of sub-millimeter in-plane spatial resolution [23]Na MRI in skin at clinically acceptable acquisition times at 7.0 T. Intra-subject variability of human skin sodium content in the volunteer population was <10.3%. An age-dependent increase in skin Na^+ content was observed (r = 0.78). Assigning sodium stores with [23]Na-MRI techniques could be improved at 7.0 T compared to current 3.0 T technology.
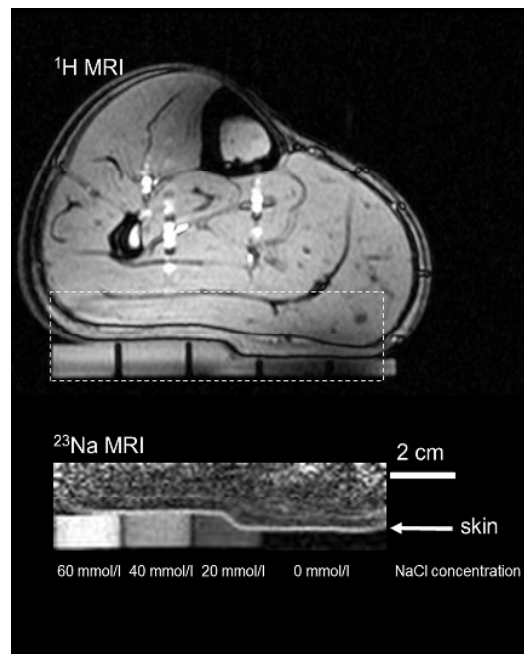
Introduction

Cardiovascular disease is the most common cause of death worldwide and hypertension (high blood pressure) is the primary risk factor (1). A reduced salt intake has been moved to be the primary adjustable behavior-related variable that should be adapted by every society worldwide (2). Over 100 years ago, Wahlgren found that the skin is a major storage depot for NaCl (3). This information was subsequently largely forgotten as clinical research focused on Na^+ regulation with regards to extracellular fluid volume in terms of a two-compartment model ultimately determined by renal function (4). Ivanova et al. pointed out that the skin has a Na^+-depositing function; however, their paper was published in Russian and was not widely appreciated (5). Ashing and atomic absorption spectrometry demonstrated that the skin is an active Na^+ depot in which Na^+ is also bound to glycosaminoglycans in an osmotically inactive fraction (6,7). It was subsequently observed that monocyte phagocytic system (MPS) cells regulate this storage depot in response to a local hypertonic microenvironment (8). MPS cells harbor the tonicity-responsive-enhance binding protein (TonEBP; NFAT5) and signal lymph-capillary density via vascular endothelial growth factor-C (VEGF-C). An increase in lymph-capillary density enables Na^+ clearance from the skin and interference with this process results in salt-sensitive hypertension (9).

Sodium magnetic resonance imaging (^{23}Na MRI) constitutes a valuable approach for *in vivo* measurement of tissue Na^+ concentrations (10,11). We have developed ^{23}Na-MRI as a method to non-invasively study the Na^+ skin depot in normal and hypertensive humans (12,13). We calibrated the method with human tissue that was then ashed and measured with atomic absorption spectrometry (12). We have shown that the proposed 3.0 T approach has clinical utility (12-14).

Realizing the intrinsic sensitivity gain at higher magnetic field strengths (15-24), ^{23}Na MRI at B_0=7.0 T is conceptually appealing to enhance spatial resolution. We reasoned that at 7.0 T, the capabilities to assess Na+ in skin would provide more precision in estimating skin Na$^+$ content. For this reason this study examines the feasibility of high in-plane spatial resolution ^{23}Na MRI in skin at 7.0 T using clinically acceptable acquisition times. To meet this goal we propose a local two-element transceiver RF surface coil that is customized for skin imaging at 7.0 T. Phantom experiments are performed to carefully assess the transmission field performance of the proposed transceiver RF coil an to examine the sensitivity of the proposed 7.0 T configuration versus a 3.0 T setup. The applicability of the proposed approach for high in-plane spatial resolution ^{23}Na MRI of the skin at 7.0 T is presented and its suitability for assessment of sodium skin content is demonstrated in initial volunteer studies, as a precursor to broader clinical studies. Intra-subject variability is examined in healthy male volunteers before extra variances due to gender or pathophysiological conditions are introduced. Age dependent differences in skin Na$^+$ content are presented.

Experimental

RF coil design

To balance the competing constraints of element size, number of elements, anatomical coverage, RF depth penetration and B_1^+ efficiency a ^{23}Na transmit/receive (TX/RX) surface coil (f=78.5 MHz) was developed for assessment of skin sodium content. The planar RF coil design comprises two loop elements each with an outer loop size of 70 mm x 64 mm and a conductor width of 12 mm as outlined in Figure 1A. The small element and RF coil size and the low resonance frequency of 78.5 MHz did not require the use of an RF shield. The structure shown in Figure 1A was etched from 16 μm copper on 0.5 mm FR4 substrate. Non-magnetic ceramic capacitors (American Technical Ceramics Inc., Huntington Station, NY, USA) and non-magnetic trimmer capacitors (Voltronics Inc., Denville, NJ, USA) were used for tuning, matching and subdividing the conductor loops into sections. The loop elements were decoupled via a shared capacitor using a non-magnetic trimmer capacitor (Voltronics Inc., Denville, NJ, USA).

The RF coil casing (length: 160 mm, width: 125 mm: height: 28mm) is shown in Figure 1B. The casing accommodates the loop elements and was designed in Autodesk Inventor Professional 2012 (Autodesk Inc., San Rafael, CA, USA). The RF coil casing was made from ABS+ material using a rapid prototyping system (BST 1200es, Dimension Inc., Eden Prairie, MN, USA). The housing ensures a minimum distance of 10 mm from the current-carrying conductors to the subject's tissue.

MR hardware

MR experiments were conducted on a horizontal 7.0 T whole body system (bore size: 60 cm, Magnetom, Siemens Healthcare, Erlangen, Germany, the product is neither cleared nor approved or labelled according to applicable medical device law and may only be used in clinical studies/trials according to applicable law. Its future commercial availability cannot be ensured), equipped with an Avanto gradient system (slew rate: 200 mT/m/ms, maximum gradient strength: 45 mT/m; Siemens Medical Solutions, Erlangen, Germany) and an 8 kW single channel RF amplifier (YXLON GmbH, Stolberg-Vicht, Germany). The RF signal was split from 1 to 2 signals by means of a home-built power splitter. For this purpose a Wilkinson power splitter was used in lumped element design that features equal amplitude and zero phase outputs. Both elements were connected to the system through a multipurpose interface box equipped with transmit/receive switches and integrated low-noise preamplifiers (Stark Contrast, Erlangen, Germany) adjusted to the resonance frequency of sodium at 7.0 T.

RF safety assessment

Three dimensional electromagnetic field (EMF) simulations were conducted using the Finite Integration Technique (CST Studio Suite 2011, CST AG, Darmstadt, Germany). For EMF simulations a virtual model of the RF coil configuration - which resembles the experimental version - was used together with the calf (length 74 cm, weight 8 kg) of the human voxel model 'Duke' from the Virtual Family (IT'IS Foundation, Zuerich, Switzerland) (25). An isotropic resolution of 1.2 mm was used to establish a uniform mesh across the calculation volume. This mesh was locally refined in the area of the conductors and the skin. Decoupling capacitors were incorporated in the EMF simulations as lumped elements which were iteratively adjusted. The feeding points of the elements were modeled as 50 Ω ports.

Final field results were accomplished by incorporating lumped tuning and matching capacitors in the built-in circuit simulator of CST Studio Suite (CST Design Studio) (26). Using the results of the EMF simulations signal absorption rates (SAR) were calculated. The input power was adjusted to meet the regulations of the IEC guideline IEC 60601-2-33 Ed.3 (27). Prior to the volunteer study the RF coil underwent thorough safety assessment in line with IEC 60601-2-33:2010 Ed.3 and IEC 60601-1:2005 Ed.3 (27). The safety assessment, the implemented safety measures, the technical documentation and the risk management file for the coil were evaluated and duly approved for implementation in clinical studies following certification by a notified body. The notified body is an accredited test laboratory that is independent from manufacturer or distributor and that has been approved by an independent third party to perform tests within a defined test scope for medical devices and hence is entitled to examine whether a product or procedure complies with the requirements of a certain standard or an equivalent standard document.

Transmission field mapping

Flip angle (FA) maps were generated to measure the transmit sensitivity profile (B_1^+) of the ^{23}Na-RF coil in agarose phantoms and *in vivo*. For this purpose a 40 mmol/l NaCl cuboid phantom (dimensions 30 x 105 x 75 mm^3) was placed at the same position of the RF coil casing as the agarose standards in the volunteer studies. A double angle method (number of averages NA=200, repetition time TR = 200 ms and flip angle $FA_{1,2}$ = 45°/90°) was implemented for B_1^+ mapping of the phantom (28). A phase-based approach was used for *in vivo* B_1^+ mapping (matrix size=32x32x10, NA=12, TR = 40 ms; total acquisition time TA=307 s) to afford short TR while being immune against T_1 saturation effects (29,30). The voxel size of (4x4x10) mm^3 allowed for sufficient SNR.

Phantom Study: SNR assessment

      To validate and quantify the sensitivity gain at 7.0 T using the proposed surface coil array phantom experiments were performed at 3.0 T and 7.0 T. For this purpose three setups were employed:

- ^{23}Na MRI with a volume RF coil at 3.0 T to resemble the setup reported in recent state-of-the-art ^{23}Na MR studies (12-14).

- ^{23}Na MRI with a volume RF coil configuration at 7.0 T.

- ^{23}Na MRI with the proposed two-element RF surface coil array at 7.0 T.

    At 3.0 T phantom experiments were conducted using a 60 cm bore (Tim Trio, Siemens, Erlangen, Germany) and a 70 cm bore (Verio, Siemens, Erlangen, Germany) MR scanner. A mono-resonant ^{23}Na MR birdcage volume knee coil (inner diameter= 20.6 cm, Stark Contrast GmbH, Erlangen, Germany) was used for excitation and reception. At 7.0 T phantom experiments were conducted using a mono-resonant bird cage coil (inner diameter=18.5 cm, Stark Contrast GmbH, Erlangen, Germany) equipped with 12 rung and tailored for ^{23}Na MR. For comparison the proposed surface coil array was applied at 7.0 T. For the phantom a thin layer of foam (thickness=1 mm) saturated with 50mM NaCl was used to mimic skin. A plastic container (size=(105 x 35 x 200) mm^3) filled with 25mM NaCl (aqueous) was employed to mimic muscle. ^{23}Na MRI was performed using a 2D gradient echo pulse sequence using: TE = 2.07 ms, TR = 150 ms, FA = 90°, bandwidth = 400 Hz/pixel, FOV = (192 x 192) mm^2, matrix size = 64 x 64, voxel size (3.0 x 3.0 x 30) mm^3, number of averages: NA= 32, TA = 5.12 min. Phase encoding was applied perpendicular to the foam layer along the A-P direction. Also, for the surface coil array a high resolution 2D gradient echo ^{23}Na MRI protocol was applied using: TE = 3.47 ms, TR = 150 ms, FA = 90°, bandwidth = 310

Hz/pixel, FOV = (128 x 128) mm^2, matrix size = 128 x 128, voxel size (1.0 x 1.0 x 30) mm^3, number of averages: NA= 16, TA = 5.12 min with phase encoding being applied perpendicular to the foam layer along the A-P direction.

Volunteer study

17 healthy men aged 20 – 79 years (mean ± SD = 46 ± 18 years) were examined after due approval by the local ethical committee (registration number DE/CA73/5550/09, Landesamt für Arbeitsschutz, Gesundheitsschutz und technische Sicherheit, Berlin, Germany) and after written informed consent was obtained prior to the study.

For volunteer studies the ^{23}Na RF coil was positioned inside a ^{1}H birdcage RF coil (Siemens Healthcare, Erlangen, Germany) as depicted in Figure 1D. The ^{1}H RF coil was used for acquisition of anatomical reference images. For Na$^+$ calibration, an array of 5% agarose gels containing 0, 20, 40, and 60 mmol/l NaCl was used as an external standard. The standards were placed on top of the ^{23}Na surface RF coil. For the 20, 40, and 60 mmol/l NaCl standards dimensions of (10 x 20 x 75) mm^3 were used. The Na$^+$ free agarose compartment was thinner ((5 x 20 x 75) mm^3) to get skin tissue closer to the surface RF coil and to increase signal-to-noise ratio (SNR).

Volunteers were positioned feet-first and supine in the scanner. The posterior section of the lower left leg was positioned directly onto the external standards. External standards and the calf were carefully aligned parallel to the z axis of the scanner to obtain straight transversal slices and to reduce partial volume effects with tissue components other than skin along the head-to-feet direction. To assess the intra-subject reproducibility, each volunteer was examined three to five times with each session including a 5 min walk and repositioning/preparation of the subject. Na$^+$ signal intensities were evaluated for skin regions

positioned directly above the NaCl free agarose standard which was positioned in the region where the sensitivity of the RF coil is largest.

For anatomical reference, a proton localizer was used: 2D FLASH, echo time (TE) = 3.7 ms, repetition time (TR) = 7.7 ms, flip angle (FA) = 20°, bandwidth = 320 Hz/pixel, field of view (FOV) = (192 x 192) mm^2, slice thickness = 5 mm, matrix size = 320 x 240, interpolated voxel size (0.38 x 0.38 x 5) mm^3), total acquisition time (TA) of 1.8 s.

^{23}Na MRI was performed using a 2D gradient echo pulse sequence to leverage the point spread function advantage over non-cartesian acquisition strategies (31-33). Unlike non-cartesian acquisition strategies such as radial or projection reconstruction approaches 2D cartesian techniques run the trait that T$_2$* induced blurring occurs only along one spatial direction, which is beneficial for ^{23}Na MRI of skin using the proposed setup where the read-out direction can be aligned with the planar layer of the skin. Also, for reasons of being able to translate the proposed approach into broader in vivo studies the imaging protocol was built on a gradient echo imaging technique which is more common and robust on clinical MR scanners versus sophisticated non-cartesian approaches (34-37). The sequence was tailored for shortest TE=2.27 ms possible using a highly asymmetric echo with the echo positioned at 1/8 of the acquisition window together with a Gaussian pulse (t=400 µs) for excitation and TR = 135 ms, FA = 90°, bandwidth = 280 Hz/pixel, FOV = (128 x 128) mm^2, matrix size = 142 x 142, voxel size (0.9 x 0.9 x 30) mm^3, number of averages: NA= 32, TA ≈ 10 min. Phase encoding was applied perpendicular to the skin along the A-P direction.

To quantify Na$^+$ content, T$_1$ saturation effects were examined. For this purpose, a volunteer (67 year-old man) was scanned several times together with an agarose standard (with 40 mmol/l NaCl) using a gradient echo imaging pulse sequence (FA = 90°, bandwidth = 310 Hz/pixel, FOV = (128 x 64) mm^2, voxel size = (1 x 1 x 30) mm^3, NA = 32, TE = 3.47

ms) in conjunction with repetition times ranging from TR = 10 ms to TR = 200 ms. Also, the bi-exponential T_2* decay rates of Na+ in skin tissue and agarose standards were measured using a fast 3D radial technique (38) with TR = 200 ms, FA = 90°, bandwidth = 200 Hz/pixel, FOV = (128 x 128 x128) mm^3, voxel size = (1 x 1 x 1) mm^3, NA= 2 and with TE ranging from 0.05 ms to 20 ms. The T_2* relaxation times obtained for the fast and slowly decaying fractions of agarose and skin and their volume fraction ratio were used in a Matlab routine (MathWorks, Natick, MA, USA) to examine the signal difference for both setups when using a TE ranging from 1 ms to 10 ms including TE=2.27 ms used in the in vivo experiments.

Data Analysis

All images were processed with ImageJ software package (NIH, Bethesda, USA). For the phantom experiments conducted at 3.0 T and at 7.0 T signal to noise ratio assessment was performed using the mean signal intensity of a ROI positioned in the phantom in a 3 mm distance to the surface of the phantom divided by the standard deviation of the noise obtained from a ROI placed in the background noise of the images. For the volunteer studies the surface RF coil B_1 profile was corrected using the B_1-map derived from an agarose cuboid phantom. For this purpose, the uncorrected human skin images were divided by the B_1^- ·sin(B_1^+·FA) map with FA=90°, which was derived from the agarose phantom. This B_1 correction is justified by the low resonance frequency of the sodium for which $B_1^- \approx B_1^+$, the use of a transmit/receive RF coil (39) and the homogeneity of the large agarose phantom. No image interpolations were applied.

The mean signal intensities derived from the NaCl free agarose standard served to determine the background signal level. The ten-fold value of the background signal was

defined as a lower threshold to identify all the pixels containing skin. The portion of this region, which was located above the 0 mmol/l NaCl agarose standard was evaluated for skin Na^+ content. The dimension of the ROI perpendicular to the skin was adjusted to the dimension of the skin. The mean signal intensity of the skin was compared with the intensity values of 20, 40, and 60 mmol/l NaCl agarose phantoms in a linear trend analysis. Standard deviation of signal intensities in the skin ROI was used to define the standard deviation of Na^+ content in skin tissue. The intra-subject standard deviation was defined as the variance of successive measurements in each volunteer. To test the linear dependence of sodium content versus age, we calculated a Pearson product-moment correlation coefficient.

Results

RF coil characteristics and RF safety assessment

The RF coil weighs 340 g. Reflection coefficients of the individual elements obtained from volunteers are better than -20 dB. Element coupling was below -10 dB for all elements and subjects. Local SAR values averaged over 10g (SAR_{10g}) were derived from the EMF simulations using the human voxel models "Duke" for an accepted input power of 2 W averaged over a period of 6 min. The local SAR maxima averaged over 10g (SAR_{10g}) for phase setting 1 (PS1, channel 1: 0^0, channel 2: 0^0) did not exceed $SAR_{10g}(max)$=18.6 W/kg which is well below the limits permitted by the IEC guidelines (27). The maximum SAR limits were found close to the surface of the human calf as demonstrated by the maximum intensity projection (MIP) of SAR for an axial view of the calf shown in Figure 2A. No SAR hot spots were observed for deep lying regions in the calf (Figure 2A). The locations and amplitudes of the local SAR maxima were found to be around the middle conductor as illustrated by the maximum intensity projection of SAR for the coronal view of the calf shown in Figure 2B. The other phase settings used in the numerical simulations provided local SAR maxima values averaged over 10g (SAR_{10g}): PS2: ch1=0^0, ch2=15^0, $SAR_{10g}(max)$=18.2 W/kg; PS3: ch1=0^0, ch2=30^0, $SAR_{10g}(max)$=17.2 W/kg; PS4: ch1=0^0, ch2=45^0, $SAR_{10g}(max)$=15.9 W/kg; PS5: ch1=0^0, ch2=60^0, $SAR_{10g}(max)$=10.0 W/kg; PS6: ch1=0^0, ch2=75^0, $SAR_{10g}(max)$=11.9 W/kg; PS7: ch1=0^0, ch2=90^0; $SAR_{10g}(max)$=9.7 W/kg), which were all below averaged local 10g (SAR_{10g}) maxima obtained for PS1. With these results the RF coil underwent thorough safety assessment in line with IEC 60601-2-33:2010 Ed.3 and IEC 60601-1:2005 Ed.3 (27).

Transmission field mapping

The distribution of the transmission fields derived from B_1^+ mapping in the phantom using the proposed RF coil are shown in Figure 2C. For a transmitter voltage of 25 V the largest SNR was obtained in the central region of the coil defining a nominal flip angle of 90°, which is scaled to 1 in the B_1^+ map. The flip angle was found to decay about 50 % per 1 cm distance from the surface of the coil. The distribution of the transmission field derived from *in vivo* B_1^+ mapping using the proposed RF coil revealed a fair agreement with the phantom data as demonstrated in Figure 2C.

Phantom study: SNR assessment

Figure 3 summarizes the results derived from the phantom experiments which were conducted to assess the sensitivity gain at 7.0 T using the proposed surface coil array versus (i) a 3.0 T setup employing a transceiver volume RF coil and (ii) a 7.0 T configuration using a volume RF coil. For the 3.0 T setup an SNR of approximately 15 was obtained for the 60 cm bore and the 70 cm bore MR scanner. At 7.0 T a SNR of approximately 50 was found when using the birdcage volume RF coil. In comparison an SNR of approximately 140 was observed when employing the proposed two-element RF surface coil configuration. These results indicate an order of magnitude improvement in SNR when moving from using a volume at 3.0 T to a RF surface coil array tailored for ^{23}Na MR of skin at 7.0 T. This sensitivity gain was translated into the high spatial resolution which indicates an improved delineation of the boundaries of the thin foam layer due to reduction in partial volume effects while keeping the scan time constant. The high spatial resolution protocol revealed an SNR of approximately 22.

Volunteer study

The proton images served for anatomical orientation to optimize skin positioning and field of view adjustments for sodium imaging as outlined in Figure 4A.

T_1 saturation effects of human skin ($T_1 = 27 \pm 2$ ms) were found to be similar to that of 50 mmol/l NaCl in 5 % agarose ($T_1 = 20 \pm 2$ ms). Consequently, we used agarose as an external standard to afford repetition times without compromising the spin density weighting needed for Na^+ calibration. At TR > 100 ms the error in concentration calibration for skin using agarose standards was well below 5 %. It was more challenging to reduce if not eliminate T_2^* contributions to the signal intensity. In vivo ^{23}Na T_2^* mapping of the skin using a fast 3D radial technique yielded a bi-exponential T_2^* decay ($R^2 > 0.99$) including a fast and a slow component with $T_2^*_{fast} = (0.5 \pm 0.3)$ ms (volume fraction=14%) and $T_2^*_{slow} = (7.6 \pm 0.5)$ ms (volume fraction=86%). To minimize T_2^* related contributions to the calibration, external agarose standards mimicking the T_2^* relaxation properties of tissue were used ($T_2^*_{fast} = 2.3 \pm 0.5$ ms, 43%, $T_2^*_{slow} = 13 \pm 2$ ms, 57%). With this setup our simulations showed a difference of less than 1% in the T_2^* effect between the agarose standard and the skin for TE=2.27 ms used in the volunteer study. The agarose standards employed here exhibit dielectric properties, which resemble those of human skin.

Imaging with the ^{23}Na RF coil provided a high in-plane spatial resolution of (0.9 x 0.9) mm^2 as illustrated in Figure 4B. The signal intensities of the 20, 40, and 60 mmol/l Na^+-standards could be very well distinguished from each other. The Na^+ signal in the thin skin layer showed high contrast versus the 0 mmol/l NaCl agarose (Figure 3B). The skin layer was very well delineated from the subcutaneous fat tissue layer. Normalization of the Na^+-image with the flip angle map removed B_1 inhomogeneities as demonstrated in Figure 4C. Consequently, intensity values of the external Na^+ standards could be compared with the

mean signal intensity of the skin in a linear trend analysis. A Na^+ content ranging from approximately 30 mmol/l to approximately 60 mmol/l was detected for the normal subjects included in the study. This range of Na^+ content covers the linear segment of the calibration curve (12,13).

The intra-subject variability of skin Na^+ content assessment was found to be below 10.3% for all subjects as demonstrated in Figure 5. The volunteer studies revealed inter-volunteer differences in skin Na^+ content. For example, the skin Na^+ content of a 25 year-old man was found to be 41 ± 2 mmol/l as depicted in Figure 6A. In comparison, a 67 year-old man showed a skin Na^+ content which was approximately 1.4-fold higher (57 ± 3 mmol/l) as illustrated in Figure 6B. Our [23]Na MRI *in vivo* data suggested an age-dependent increase in the skins Na^+ content as illustrated in Figure 7. The relationship could be represented by a linear fit with a slope of (0.34 ± 0.07) mmol/(l·year). For the linear dependence of sodium content versus age a Pearson product-moment correlation coefficient of r = 0.78 was observed.

Discussion

The important findings in our study are that ^{23}Na-MRI has utility in measuring compartmentalized Na$^+$ stores in skin that exceed hitherto forwarded methodologies. The evidence herein suggests that ^{23}Na-MRI at 7.0 T provides sensitivity and spatial resolution advantages over a recent 3.0 T study (13). The same study concluded that further technological advancements in the field are required to provide more spatially detailed images of the skin. This conclusion prompted the authors to propose the use of 7.0 T MRI. Our study adds to the literature by demonstrating the feasibility of high spatial resolution human skin ^{23}Na MR at 7.0 T. With ^{23}Na MRI at 7.0 T we observed that the sensitivity of the proposed RF surface coil enabled the acquisition of ^{23}Na MR images at an in-plane resolution below 1 mm in the thin layer of the skin. This resolution reveals the enormous Na$^+$ content of the human skin

Taking the in-plane spatial resolution of (0.9 x 0.9) mm^2 into account and considering inter-volunteer changes in skin thickness, the skin layer was covered by 2-4 pixels in this study. Partial volume effects might systematically hamper the absolute Na$^+$ concentration but have a minor influence on the ratio from patient to patient. This situation manifests itself by the low intra-volunteer variance. It should be noted that residual partial volume effects are significantly lower compared to previous results reported for 3.0 T ^{23}Na MRI in skin (12-14). These improvements were achieved by using an enhanced in-plane spatial resolution resulting in voxels sizes being by an order of magnitude reduced versus human skin ^{23}Na MR at 3.0 T (12-14). The gain in spatial resolution was afforded by the SNR gain inherent to ultrahigh magnetic fields and by the use of a local transceiver RF coil versus birdcage RF volume coils previously applied at 3.0 T (12-14). The SNR increase observed at 7.0 T using a volume RF coil versus the equivalent setup at 3.0 T accords with previous reports on magnetic field

dependent brain ^{23}Na MR (40). The sensitivity gain obtained at 7.0 T together with the proposed local transceiver RF coil array versus the birdcage RF volume coil suggests that the use of a local transceiver RF coil array at 3.0 T would afford a factor of 3 reduction in voxel size versus previous reports about human skin ^{23}Na MR at 3.0 T (12-14).

Our *in vivo* studies in healthy subjects revealed an increased skin Na$^+$ concentration with advancing age. This finding is in alignment with a recent *in vivo* study performed at 3.0 T (13), which reported a sodium content of the skin ranging from approximately 15 mmol/L (age 22) to approximately 35 mmol/L (age 80) for a normotensive cohort of male subjects. In comparison, our results reported here demonstrated an increase in the sodium concentration of skin from approximately 35 mmol/L (age 20) to approximately 60mmol/L (age 80). This MR based range of *in vivo* skin sodium content matches ex vivo 3.0 T findings obtained for dissected skin specimens placed in a falcon tube with a diameter of 27 mm (12). The discrepancy between sodium skin content obtained *in vivo* at 3.0 T versus 7.0 T can be most likely attributed to the enhanced spatial resolution at 7.0 T which helps to offset partial volume effects encountered at lower fields.

The results reported for this feasibility study are likely to pave the way for further advances in RF coil technology tailored for assessment of skin sodium content. These efforts will help to further gain sensitivity by reducing loop element size and by including more loop elements as recently demonstrated for transceiver arrays customized for proton MRI at 7.0 T (41-46), and hence will contribute to further improvements of in-plane resolution. The use of a large slice thickness for transversal slices of skin in the lower leg implies perfect orientation of the calf-skin and agarose standards parallel to the main axis of the MR scanner to reduce partial volume effects of skin Na$^+$ signal, Na$^+$ free environment and low Na$^+$ subcutaneous fat tissue. To this end, the relatively large slice thickness used in this feasibility study could be

also reduced. This would afford an enhanced robustness and improved ease of use for clinical sodium skin content assessment.

We believe that the observation of age dependent sodium concentration in the skin is interesting, since blood pressure and hypertension increase relentlessly with age and Na^+ has been implicated mechanistically. However, we are aware that NaCl balance investigations, studies in hypertensive subjects, and determinations in patients with abnormal Na^+ concentrations will be necessary to establish the clinical utility of this imaging technique. To this end longitudinal [23]Na MR studies hold the promise to provide means for further explorations into the regulation of skin sodium storage. [35]Cl MRI presents a supplementary and very much intriguing alternative for research into salt homeostasis (47,48). Another development that is looming on the research horizon is the move toward magnetic field strengths of $B_0 = 9.4$ T and higher which will afford further spatial resolution enhancements for quantitative sodium imaging (49).

We recognized limitations in our study. A Cartesian gradient-echo technique was applied, which was optimized to the geometry and requirements of the *in vivo* setup. Further developments might include fast 2D or 3D projection reconstruction or other non-Cartesian imaging techniques (38,50-52). These approaches make use of ultra-short echo times to preserve signal of fast decaying [23]Na components and hence would help to further reduce T_2^* effects. Because of the physiological relevance of the intra- versus the extracellular Na^+ compartment, a separation between these pools constitutes another goal for the development of [23]Na-MRI techniques employing relaxation-weighted imaging or multiple-quantum filtering (33,53,54). While the proposed RF coil design is tailored to accommodate the calf it can be adapted to support in vivo assessment of human skin content in body sections other than the calf.

We believe that the investigation of human Na^+ balance can benefit from state-of-the art ^{23}Na-MRI tools and should not be thoroughly investigated solely with serum measurements and 24 h urine collections but requires state-of-the art diagnostic imaging tools. Recent reports indicate that macrophage/vascular endothelial growth factor-C-driven extrarenal regulation of interstitial electrolyte metabolism might be relevant in humans with salt-sensitive hypertension, refractory hypertension, and in patients with renal disease (8,55,56). However, non-invasive imaging approaches for quantification of interstitial Na^+ storage in humans were not available to carefully validate these assumptions. We suggest that ^{23}Na-MRI at 7.0 T can help to unlock questions regarding Na^+ balance and Na^+ storage functions of skin with the ultimate goal to provide imaging means for diagnostics and for guiding treatment decisions in cardiovascular and metabolic diseases.

Acknowledgements

References:

1. Lawes CM, Vander Hoorn S, Rodgers A, International Society of H. Global burden of blood-pressure-related disease, 2001. Lancet 2008;371(9623):1513-1518.

2. Cook NR, Appel LJ, Whelton PK. Lower levels of sodium intake and reduced cardiovascular risk. Circulation 2014;129(9):981-989.

3. Wahlgren V. Uber die Bedeutung der Gewebe als Chlordepots. Edited by R Magnus in Utrecht 1909;IX:97-112.

4. Guyton AC, Granger HJ, Coleman TG. Autoregulation of the total systemic circulation and its relation to control of cardiac output and arterial pressure. Circ Res 1971;28:Suppl 1:93-97.

5. Ivanova LN, Archibasova VK, Shterental I. [Sodium-depositing function of the skin in white rats]. Fiziol Zh SSSR Im I M Sechenova 1978;64(3):358-363.

6. Titze J, Lang R, Ilies C, Schwind KH, Kirsch KA, Dietsch P, Luft FC, Hilgers KF. Osmotically inactive skin Na+ storage in rats. Am J Physiol Renal Physiol 2003;285(6):F1108-1117.

7. Titze J, Shakibaei M, Schafflhuber M, Schulze-Tanzil G, Porst M, Schwind KH, Dietsch P, Hilgers KF. Glycosaminoglycan polymerization may enable osmotically inactive Na+ storage in the skin. Am J Physiol Heart Circ Physiol 2004;287(1):H203-208.

8. Machnik A, Neuhofer W, Jantsch J, Dahlmann A, Tammela T, Machura K, Park JK, Beck FX, Muller DN, Derer W, Goss J, Ziomber A, Dietsch P, Wagner H, van Rooijen N, Kurtz A, Hilgers KF, Alitalo K, Eckardt KU, Luft FC, Kerjaschki D, Titze J. Macrophages regulate salt-dependent volume and blood pressure by a vascular endothelial growth factor-C-dependent buffering mechanism. Nat Med 2009;15(5):545-552.

9. Wiig H, Schroder A, Neuhofer W, Jantsch J, Kopp C, Karlsen TV, Boschmann M, Goss J, Bry M, Rakova N, Dahlmann A, Brenner S, Tenstad O, Nurmi H, Mervaala E, Wagner H, Beck FX, Muller DN, Kerjaschki D, Luft FC, Harrison DG, Alitalo K, Titze J. Immune cells control skin lymphatic electrolyte homeostasis and blood pressure. J Clin Invest 2013;123(7):2803-2815.

10. Madelin G, Regatte RR. Biomedical applications of sodium MRI in vivo. J Magn Reson Imaging 2013;38(3):511-529.

11.   Konstandin S, Schad LR. 30 years of sodium/X-nuclei magnetic resonance imaging. MAGMA 2014;27(1):1-4.

12.   Kopp C, Linz P, Wachsmuth L, Dahlmann A, Horbach T, Schofl C, Renz W, Santoro D, Niendorf T, Muller DN, Neininger M, Cavallaro A, Eckardt KU, Schmieder RE, Luft FC, Uder M, Titze J. (23)Na magnetic resonance imaging of tissue sodium. Hypertension 2012;59(1):167-172.

13.   Kopp C, Linz P, Dahlmann A, Hammon M, Jantsch J, Muller DN, Schmieder RE, Cavallaro A, Eckardt KU, Uder M, Luft FC, Titze J. 23Na magnetic resonance imaging-determined tissue sodium in healthy subjects and hypertensive patients. Hypertension 2013;61(3):635-640.

14.   Dahlmann A, Dorfelt K, Eicher F, Linz P, Kopp C, Mossinger I, Horn S, Buschges-Seraphin B, Wabel P, Hammon M, Cavallaro A, Eckardt KU, Kotanko P, Levin NW, Johannes B, Uder M, Luft FC, Muller DN, Titze JM. Magnetic resonance-determined sodium removal from tissue stores in hemodialysis patients. Kidney Int 2014.

15.   Ladd ME. High-field-strength magnetic resonance: potential and limits. Top Magn Reson Imaging 2007;18(2):139-152.

16.   Regatte RR, Schweitzer ME. Ultra-high-field MRI of the musculoskeletal system at 7.0T. J Magn Reson Imaging 2007;25(2):262-269.

17.   Niendorf T, Sodickson DK, Krombach GA, Schulz-Menger J. Toward cardiovascular MRI at 7 T: clinical needs, technical solutions and research promises. Eur Radiol 2010;20(12):2806-2816.

18.   Ugurbil K. The road to functional imaging and ultrahigh fields. Neuroimage 2012;62(2):726-735.

19.   Moser E, Stahlberg F, Ladd ME, Trattnig S. 7-T MR--from research to clinical applications? NMR Biomed 2012;25(5):695-716.

20.   Trattnig S, Zbyn S, Schmitt B, Friedrich K, Juras V, Szomolanyi P, Bogner W. Advanced MR methods at ultra-high field (7 Tesla) for clinical musculoskeletal applications. Eur Radiol 2012;22(11):2338-2346.

21.   van der Kolk AG, Hendrikse J, Zwanenburg JJ, Visser F, Luijten PR. Clinical applications of 7 T MRI in the brain. Eur J Radiol 2013;82(5):708-718.

22.   Niendorf T, Graessl A, Thalhammer C, Dieringer MA, Kraus O, Santoro D, Fuchs K, Hezel F, Waiczies S, Ittermann B, Winter L. Progress and promises of human cardiac

magnetic resonance at ultrahigh fields: a physics perspective. J Magn Reson 2013;229:208-222.

23.   Kraff O, Fischer A, Nagel AM, Monninghoff C, Ladd ME. MRI at 7 tesla and above: Demonstrated and potential capabilities. J Magn Reson Imaging 2014, doi: 10.1002/jmri.24573. [Epub ahead of print]

24.   Ugurbil K. Magnetic resonance imaging at ultrahigh fields. IEEE Trans Biomed Eng 2014;61(5):1364-1379.

25.   Christ A, Kainz W, Hahn EG, Honegger K, Zefferer M, Neufeld E, Rascher W, Janka R, Bautz W, Chen J. The Virtual Family—development of surface-based anatomical models of two adults and two children for dosimetric simulations. Physics in medicine and biology 2010;55:N23.

26.   Kozlov M, Turner R. Fast MRI coil analysis based on 3-D electromagnetic and RF circuit co-simulation. Journal of Magnetic Resonance 2009;200(1):147-152.

27.   IEC. 60601-2-33 Medical electrical equipment - Part 2-33: Particular requirements for the basic safety and essential performance of magnetic resonance equipment for medical diagnosis. 3.0 ed; 2010.

28.   Akoka S, Franconi F, Seguin F, Le Pape A. Radiofrequency map of an NMR coil by imaging. Magn Reson Imaging 1993;11(3):437-441.

29.   Allen SP, Morrell GR, Peterson B, Park D, Gold GE, Kaggie JD, Bangerter NK. Phase-sensitive sodium B1 mapping. Magn Reson Med 2011;65(4):1125-1130.

30.   Carinci F, Santoro D, von Samson-Himmelstjerna F, Lindel TD, Dieringer MA, Niendorf T. Characterization of phase-based methods used for transmission field uniformity mapping: a magnetic resonance study at 3.0 T and 7.0 T. PLoS One 2013;8(3):e57982.

31.   Rahmer J, Bornert P, Groen J, Bos C. Three-dimensional radial ultrashort echo-time imaging with T2 adapted sampling. Magn Reson Med 2006;55(5):1075-1082.

32.   Nagel AM, Weber M-A, Wolf MB, Semmler W. 3D density-adapted projection reconstruction 23Na-MRI with anisotropic resolution and field-of-view. 2012; Melbourne, Australia. p 2282.

33.   Konstandin S, Nagel AM. Measurement techniques for magnetic resonance imaging of fast relaxing nuclei. MAGMA 2014;27(1):5-19.

34.   Noebauer-Huhmann IM, Juras V, Pfirrmann CW, Szomolanyi P, Zbyn S, Messner A, Wimmer J, Weber M, Friedrich KM, Stelzeneder D, Trattnig S. Sodium MR imaging of the lumbar intervertebral disk at 7 T: correlation with T2 mapping and modified Pfirrmann score at 3 T--preliminary results. Radiology 2012;265(2):555-564.

35.   Juras V, Zbyn S, Pressl C, Domayer SE, Hofstaetter JG, Mayerhoefer ME, Windhager R, Trattnig S. Sodium MR imaging of Achilles tendinopathy at 7 T: preliminary results. Radiology 2012;262(1):199-205.

36.   Haneder S, Juras V, Michaely HJ, Deligianni X, Bieri O, Schoenberg SO, Trattnig S, Zbyn S. In vivo sodium (23Na) imaging of the human kidneys at 7 T: preliminary results. Eur Radiol 2014;24(2):494-501.

37.   Zbyn S, Mlynarik V, Juras V, Szomolanyi P, Trattnig S. Sodium MR Imaging of Articular Cartilage Pathologies. Curr Radiol Rep 2014;2:41.

38.   Nielles-Vallespin S, Weber MA, Bock M, Bongers A, Speier P, Combs SE, Wohrle J, Lehmann-Horn F, Essig M, Schad LR. 3D radial projection technique with ultrashort echo times for sodium MRI: clinical applications in human brain and skeletal muscle. Magn Reson Med 2007;57(1):74-81.

39.   Glover GH, Hayes CE, Pelc NJ, Edelstein WA, Mueller M, Hart HR, Hardy CJ, O'Donnell M, Barber WD. Comparison of Linear and Circular Polarization for Magnetic Resonance Imaging. Semin Dial 1985;64(1):255-270.

40.   Nagel AM, Schmitter S, Bock M, Moser E, Semmler W, Schad LR. Parameter optimization for 7T 23Na-MRI. in Proceedings of 17th Annual Meeting of the International Society of Magnetic Resonance in Medicine 2009:2465.

41.   Dieringer MA, Renz W, Lindel T, Seifert F, Frauenrath T, von Knobelsdorff-Brenkenhoff F, Waiczies H, Hoffmann W, Rieger J, Pfeiffer H, Ittermann B, Schulz-Menger J, Niendorf T. Design and application of a four-channel transmit/receive surface coil for functional cardiac imaging at 7T. J Magn Reson Imaging 2011;33(3):736-741.

42.   Grassl A, Winter L, Thalhammer C, Renz W, Kellman P, Martin C, von Knobelsdorff-Brenkenhoff F, Tkachenko V, Schulz-Menger J, Niendorf T. Design, evaluation and application of an eight channel transmit/receive coil array for cardiac MRI at 7.0 T. Eur J Radiol 2013;82(5):752-759.

43.	Thalhammer C, Renz W, Winter L, Hezel F, Rieger J, Pfeiffer H, Graessl A, Seifert F, Hoffmann W, von Knobelsdorff-Brenkenhoff F, Tkachenko V, Schulz-Menger J, Kellman P, Niendorf T. Two-dimensional sixteen channel transmit/receive coil array for cardiac MRI at 7.0 T: design, evaluation, and application. J Magn Reson Imaging 2012;36(4):847-857.

44.	Winter L, Kellman P, Renz W, Grassl A, Hezel F, Thalhammer C, von Knobelsdorff-Brenkenhoff F, Tkachenko V, Schulz-Menger J, Niendorf T. Comparison of three multichannel transmit/receive radiofrequency coil configurations for anatomic and functional cardiac MRI at 7.0T: implications for clinical imaging. Eur Radiol 2012;22(10):2211-2220.

45.	Graessl A, Muhle M, Schwerter M, Rieger J, Oezerdem C, Santoro D, Lysiak D, Winter L, Hezel F, Waiczies S, Guthoff RF, Falke K, Hosten N, Hadlich S, Krueger PC, Langner S, Stachs O, Niendorf T. Ophthalmic magnetic resonance imaging at 7 T using a 6-channel transceiver radiofrequency coil array in healthy subjects and patients with intraocular masses. Invest Radiol 2014;49(5):260-270.

46.	Graessl A, Renz W, Hezel F, Dieringer MA, Winter L, Oezerdem C, Rieger J, Kellman P, Santoro D, Lindel TD, Frauenrath T, Pfeiffer H, Niendorf T. Modular 32-channel transceiver coil array for cardiac MRI at 7.0T. Magn Reson Med 2014;72(1):276-290.

47.	Nagel AM, Lehmann-Horn F, Weber MA, Jurkat-Rott K, Wolf MB, Radbruch A, Umathum R, Semmler W. In Vivo Cl MR Imaging in Humans: A Feasibility Study. Radiology 2014:131725.

48.	Baier S, Kramer P, Grudzenski S, Fatar M, Kirsch S, Schad LR. Chlorine and sodium chemical shift imaging during acute stroke in a rat model at 9.4 Tesla. MAGMA 2014;27(1):71-79.

49.	Mirkes CC, Hoffmann J, Shajan G, Pohmann R, Scheffler K. High-resolution quantitative sodium imaging at 9.4 tesla. Magn Reson Med 2014.

50.	Boada FE, Gillen JS, Shen GX, Chang SY, Thulborn KR. Fast three dimensional sodium imaging. Magn Reson Med 1997;37(5):706-715.

51.	Romanzetti S, Halse M, Kaffanke J, Zilles K, Balcom BJ, Shah NJ. A comparison of three SPRITE techniques for the quantitative 3D imaging of the 23Na spin density on a 4T whole-body machine. J Magn Reson 2006;179(1):64-72.

52. Nagel AM, Laun FB, Weber MA, Matthies C, Semmler W, Schad LR. Sodium MRI using a density-adapted 3D radial acquisition technique. Magn Reson Med 2009;62(6):1565-1573.

53. Nagel AM, Bock M, Hartmann C, Gerigk L, Neumann JO, Weber MA, Bendszus M, Radbruch A, Wick W, Schlemmer HP, Semmler W, Biller A. The potential of relaxation-weighted sodium magnetic resonance imaging as demonstrated on brain tumors. Invest Radiol 2011;46(9):539-547.

54. Fiege DP, Romanzetti S, Mirkes CC, Brenner D, Shah NJ. Simultaneous single-quantum and triple-quantum-filtered MRI of 23Na (SISTINA). Magn Reson Med 2013;69(6):1691-1696.

55. Liu F, Mu J, Yuan Z, Lian Q, Zheng S, Wu G, Liu E. Involvement of the lymphatic system in salt-sensitive hypertension in humans. Med Sci Monit 2011;17(10):CR542-546.

56. Slagman MC, Kwakernaak AJ, Yazdani S, Laverman GD, van den Born J, Titze J, Navis G. Vascular endothelial growth factor C levels are modulated by dietary salt intake in proteinuric chronic kidney disease patients and in healthy subjects. Nephrol Dial Transplant 2012;27(3):978-982.

Figure Captions

Figure 1: (A) The basic design and layout of the two-element transmit/receive surface RF coil proposed for in vivo ^{23}Na MRI of the human skin at 7.0 T. **(B)** Photograph of the coil casing and cabling. **(C)** Schematic view of the positioning of the ^{23}Na surface coil with respect to the calf. For the in vivo experiments subjects were positioned feet-first and supine with the calf resting on the RF coil as illustrated by the transparent view. **(D)** Positioning of the ^{23}Na surface-coil in a ^{1}H birdcage-coil used for acquisition of anatomical reference images. For concentration calibration agarose phantoms with 0, 20, 40 and 60 mmol/l NaCl concentration were mounted on top of the ^{23}Na coil.

Figure 2: Maximum intensity projection of local SAR maxima values averaged over 10g (SAR_{10g}) for transverse **(A)** slice and for a coronal slice (B) across the calf for an input power of 2W_{rms}. SAR_{10g} distribution was derived from EMF simulations using the human voxel model "Duke". The maximum local SAR_{10g} did not exceed $SAR_{10g}(max)$=18.6 W/kg which is well below the limits permitted by the IEC guidelines (27). **C)** B_1-maps derived from phantom and volunteer studies. **top):** High resolution normalized B_1 map derived from a 40 mmol/l NaCl agarose phantom used for spatial sensitivity calibration. The map shows high sensitivity near the surface of the coil. The flip angle decays to about the half at a distance of 1 cm from the surface. **bottom):** Low spatial resolution normalized *in vivo* B_1 map of human calf. Phantom and *in vivo* B_1 maps show a fair agreement.

Figure 3: Summary of the SNR assessment derived from ^{23}Na MRI phantom experiments at 3.0 T and 7.0 T. Three setups were employed: **(i)** volume RF coil at 3.0 T using an MR scanner with a 60 cm bore **(A)** and a 70 cm bore **(B)** to resemble the setup reported in recent state-of-the-art ^{23}Na MR studies (12,13), **(ii)** a volume RF coil configuration at 7.0 T using a birdcage RF coil **(C)**, and the proposed two-element transceiver RF coil array **(D)**. The imaging protocol was adjusted **(A-D)**: to achieve an in-plane spatial resolution of (3.0 x 3.0) mm^3 reported for state-of-the-art ^{23}Na MR studies (12,13) and **(E):** to facilitate an in-plane spatial resolution of (1.0 x 1.0) mm^3 while keeping the total scan time constant. SNR was determined for a region of interest placed in the phantom (marked in red) containing 25mM NaCl to resemble skin. For the 3.0 T setup an SNR of approximately 15 was obtained for the 60 cm bore **(A)** and the 70 cm bore **(B)** MR scanner. At 7.0 T a SNR of approximately 50 was found when using the birdcage volume RF coil **(C)**. In comparison an SNR of approximately 140 was observed when employing the proposed two-element transceiver RF coil **(D)**. For the latter the high resolution protocol **(E)** yielded an SNR of approximately 22.

Figure 4: Proton image and sodium images of human calf skin acquired at 7.0 T. **(A)** Proton images served for anatomical orientation of the lower leg that was placed on an array of agarose gel standards with different NaCl concentrations of 0, 20, 40, and 60 mmol/l (from the right to the left). The dashed line surrounds the field of view of the ^{23}Na image. The ^{23}Na surface coil is positioned below the agarose standards. **(B)** ^{23}Na gradient echo image of skin. The bright white line represents the high Na concentration in the skin layer. **(C)** After normalization of the ^{23}Na MR image shown in B, the external standards can be used for calibration of tissue Na$^+$ content. Arrows indicate the position of the skin (male volunteer, 37 years)**.**

Figure 5: Intra-subject reproducibility of skin Na$^+$ acquisitions in 17 healthy subjects of increasing ages (to the right and downwards). The intra-subject variability of the human skin Na$^+$ content was below 10.3 % for all subjects.

Figure 6: ^{1}H /^{23}Na MR images of the human calf skin for volunteers with different age. **(A)** ^{1}H image (top) and ^{23}Na-MR image (bottom) derived from the lower right leg of a 25 year-old male subject. **(B)** ^{1}H image (top) and ^{23}Na MR image (bottom) derived from a 67 year-old male subject for the same slice position used in A. Anatomical structures including the subtle skin layer are visualized in the ^{1}H images. The zoomed views of the density corrected ^{23}Na images **(bottom)** represent the regions highlighted by the white boxes in the anatomical images **(top)**. Skin (marked by arrows) is very well delineated in the ^{23}Na MR images, which also show the agarose gel standards with increasing Na$^+$ content.

Figure 7: Human skin Na$^+$ content versus age obtained from ^{23}Na MRI at 7.0 T. The preliminary *in vivo* ^{23}Na MRI data (n=17, male) suggest an increase of skin Na$^+$ content with age of (0.34 ± 0.07) mmol/(l·year).
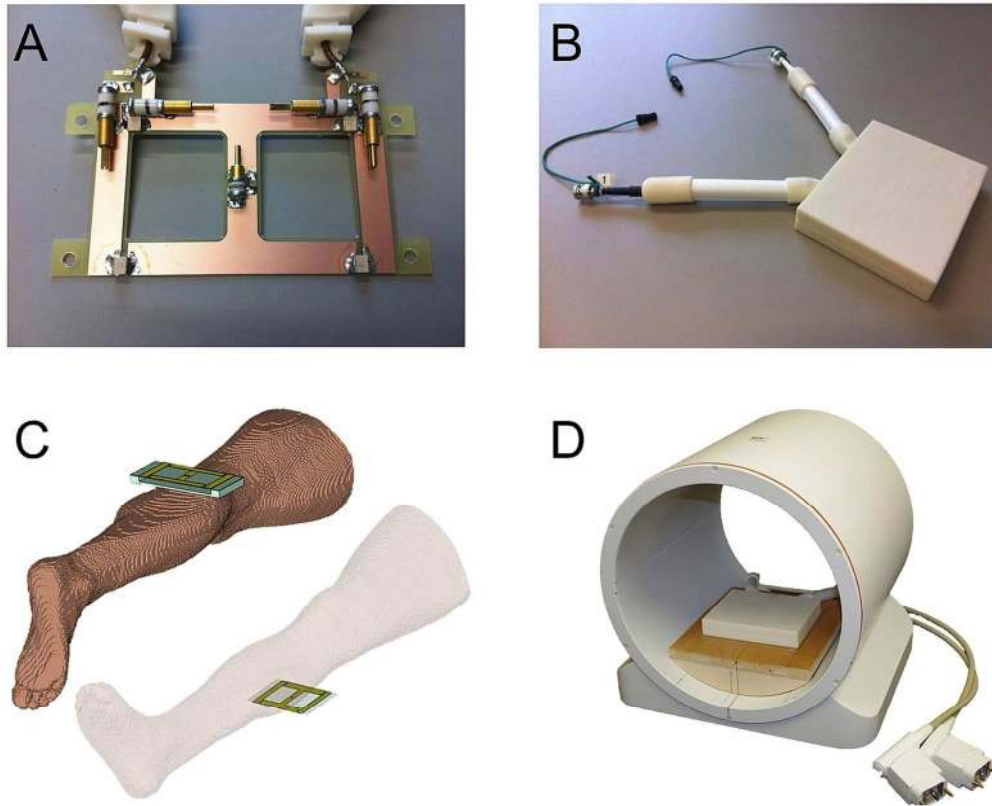
Figure 1: (A) The basic design and layout of the two-element transmit/receive surface RF coil proposed for in vivo ^{23}Na MRI of the human skin at 7.0 T. (B) Photograph of the coil casing and cabling. (C) Schematic view of the positioning of the ^{23}Na surface coil with respect to the calf. For the in vivo experiments subjects were positioned feet-first and supine with the calf resting on the RF coil as illustrated by the transparent view. (D) Positioning of the ^{23}Na surface-coil in a ^{1}H birdcage-coil used for acquisition of anatomical reference images. For concentration calibration agarose phantoms with 0, 20, 40 and 60 mmol/l NaCl concentration were mounted on top of the ^{23}Na coil.
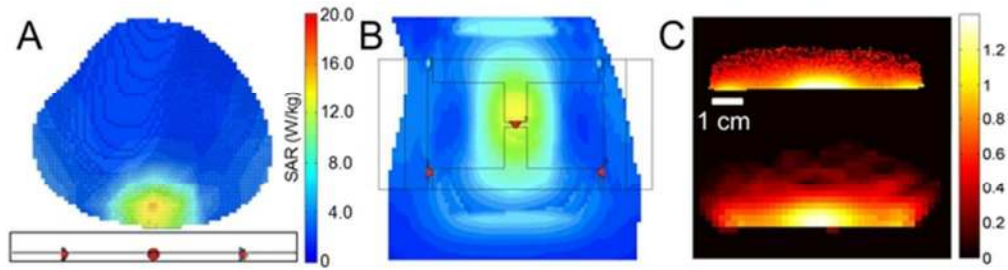161x130mm (300 x 300 DPI)

Figure 2: Maximum intensity projection of local SAR maxima values averaged over 10g (SAR_{10g}) for transverse (A) slice and for a coronal slice (B) across the calf for an input power of $2W_{rms}$. SAR_{10g} distribution was derived from EMF simulations using the human voxel model "Duke". The maximum local SAR_{10g} did not exceed $SAR_{10g}(max)=18.6$ W/kg which is well below the limits permitted by the IEC guidelines (26). C) B_1-maps derived from phantom and volunteer studies. top): High resolution normalized B_1 map derived from a 40 mmol/l NaCl agarose phantom used for spatial sensitivity calibration. The map shows high sensitivity near the surface of the coil. The flip angle decays to about the half at a distance of 1 cm from the surface. bottom): Low spatial resolution normalized in vivo B_1 map of human calf. Phantom and *in vivo* B_1 maps show a fair agreement.
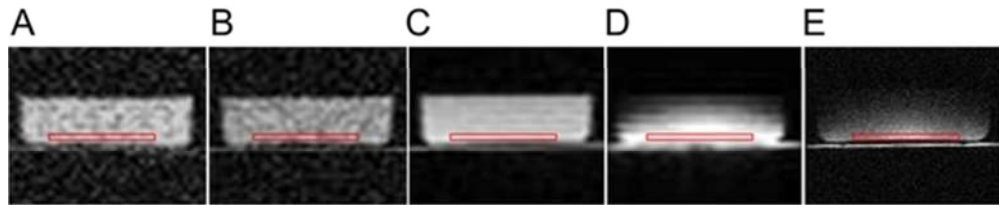55x15mm (300 x 300 DPI)

Figure 3:
Summary of the SNR assessment derived from ^{23}Na MRI phantom experiments at 3.0 T and 7.0 T. Three setups were employed: (i) volume RF coil at 3.0 T using an MR scanner with a 60 cm bore (A) and a 70 cm bore (B) to resemble the setup reported in recent state-of-the-art ^{23}Na MR studies (12,13), (ii) a volume RF coil configuration at 7.0 T using a birdcage RF coil (C), and the proposed two-element transceiver RF coil array (D). The imaging protocol was adjusted (A-D): to achieve an in-plane spatial resolution of (3.0 x 3.0) mm^3 reported for state-of-the-art ^{23}Na MR studies (12,13) and (E): to facilitate an in-plane spatial resolution of (1.0 x 1.0) mm^3 while keeping the total scan time constant. SNR was determined for a region of interest placed in the phantom (marked in red) containing 25mM NaCl to resemble skin. For the 3.0 T setup an SNR of approximately 15 was obtained for the 60 cm bore (A) and the 70 cm bore (B) MR scanner. At 7.0 T a SNR of approximately 50 was found when using the birdcage volume RF coil (C). In comparison an SNR of approximately 140 was observed when employing the proposed two-element transceiver RF coil (D). For the latter the high resolution protocol (E) yielded an SNR of approximately 22.
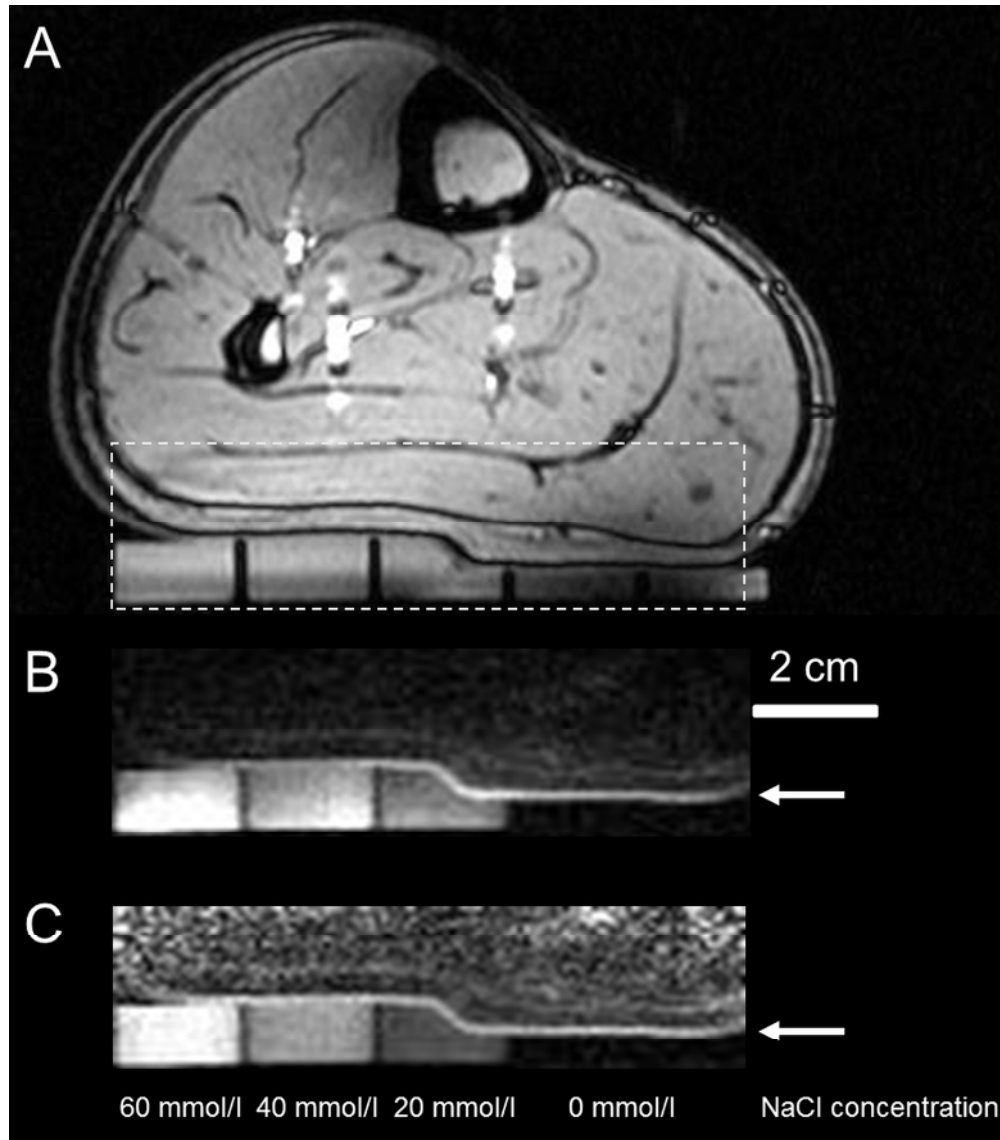49x12mm (300 x 300 DPI)

Figure 4:
Proton image and sodium images of human calf skin acquired at 7.0 T. (A) Proton images served for anatomical orientation of the lower leg that was placed on an array of agarose gel standards with different NaCl concentrations of 0, 20, 40, and 60 mmol/l (from the right to the left). The dashed line surrounds the field of view of the ^{23}Na image. The ^{23}Na surface coil is positioned below the agarose standards. (B) ^{23}Na gradient echo image of skin. The bright white line represents the high Na concentration in the skin layer. (C) After normalization of the ^{23}Na MR image shown in B, the external standards can be used for calibration of tissue Na$^+$ content. Arrows indicate the position of the skin (male volunteer, 37 years).
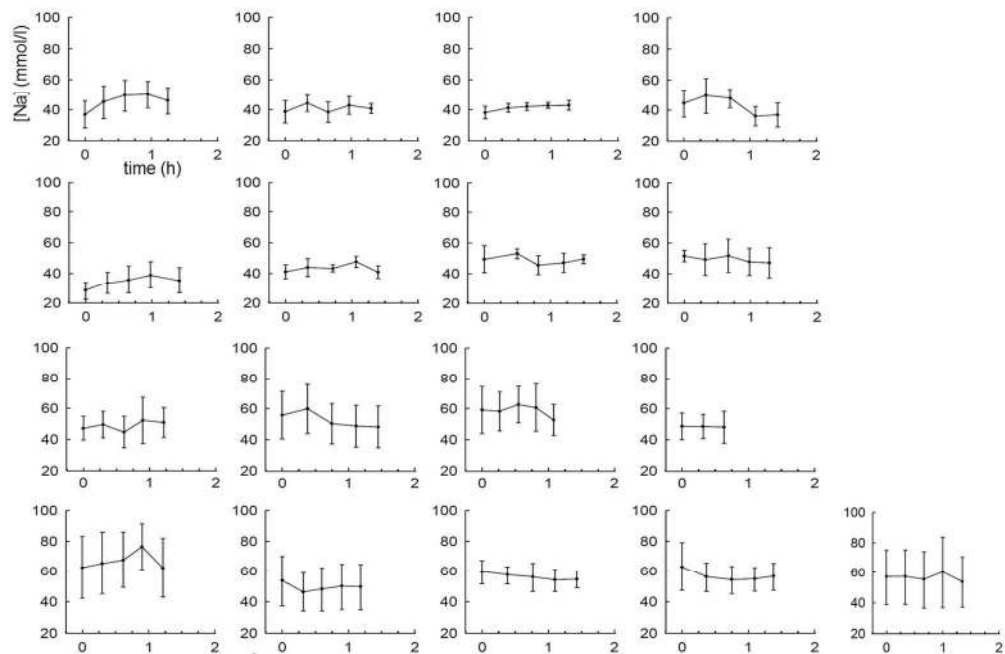113x128mm (300 x 300 DPI)

Figure 5:
Intra-subject reproducibility of skin Na+ acquisitions in 17 healthy subjects of increasing ages (to the right and downwards). The intra-subject variability of the human skin Na$^+$ content was below 10.3 % for all subjects.
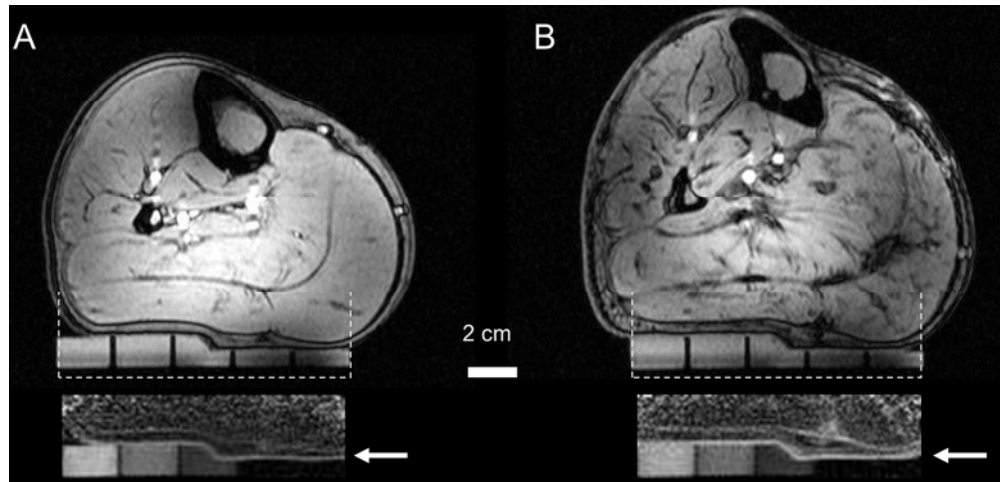133x89mm (300 x 300 DPI)

Figure 6:
[1]H /[23]Na MR images of the human calf skin for volunteers with different age. (A) ^{1}H image (top) and [23]Na-MR image (bottom) derived from the lower right leg of a 25 year-old male subject. (B) ^{1}H image (top) and [23]Na MR image (bottom) derived from a 67 year-old male subject for the same slice position used in A. Anatomical structures including the subtle skin layer are visualized in the ^{1}H images. The zoomed views of the density corrected [23]Na images (bottom) represent the regions highlighted by the white boxes in the anatomical images (top). Skin (marked by arrows) is very well delineated in the [23]Na MR images, which also show the agarose gel standards with increasing Na^+ content.
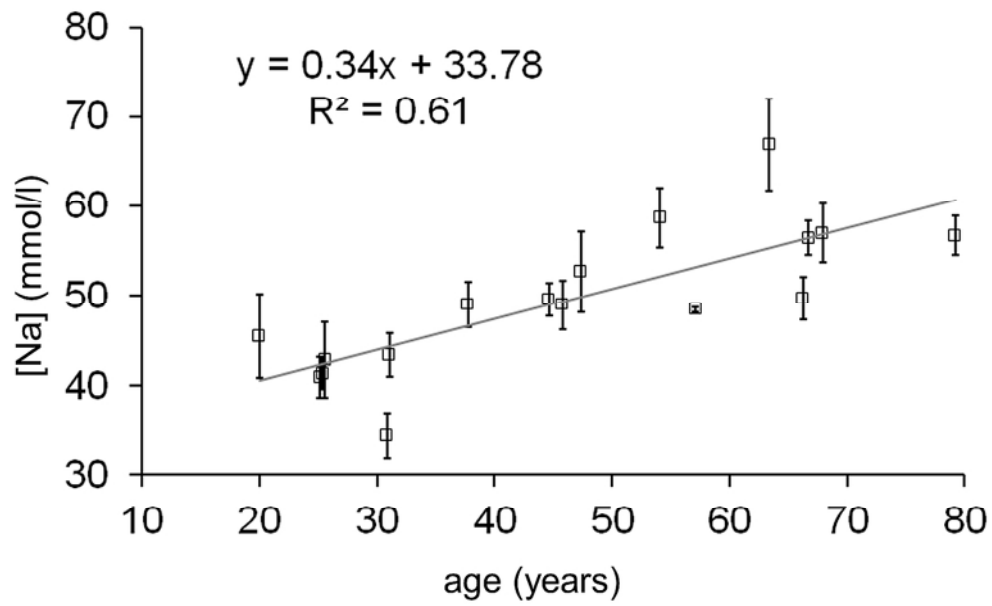96x46mm (300 x 300 DPI)

Figure 7:
Human skin Na$^+$ content versus age obtained from ^{23}Na MRI at 7.0 T. The preliminary in vivo ^{23}Na MRI data (n=17, male) suggest an increase of skin Na$^+$ content with age of (0.34 ± 0.07) mmol/(l·year).
91x56mm (300 x 300 DPI)